ACS APPLIED MATERIALS & INTERFACES

www.acsami.org

Research Article

Thermally Triggered, Cell-Specific Enzymatic Glyco-Editing: *In Situ* Regulation of Lectin Recognition and Immune Response on Target Cells

Xiaofei Yu, Huifang Shi, Yiran Li, Yuna Guo, Peiwen Zhang, Guyu Wang, Lei Li, Xian Chen, Lin Ding,* and Huangxian Ju

Cite This: *ACS Appl. Mater. Interfaces* 2020, 12, 54387−54398

Read Online

ACCESS | Metrics & More | Article Recommendations | Supporting Information

ABSTRACT: *In situ* glyco-editing on the cell surface can endow cellular glycoforms with new structures and properties; however, the lack of cell specificity and dependence on cells' endogenous functions plague the revelation of cellular glycan recognition properties and hamper the application of glyco-editing in complicated authentic biosystems. Herein, we develop a thermally triggered, cell-specific glyco-editing method for regulation of lectin recognition on target live cells in both single- and cocultured settings. The method relies on the aptamer-mediated anchoring of microgel-encapsulated neuraminidase on target cells and subsequent thermally triggered enzyme release for localized sialic acid (Sia) trimming. This temperature-based enzyme accessibility modulation strategy exempts genetic or metabolic engineering operations and, thus for the first time, enables tumor-specific desialylation on complicated tissue slices. The proposed method also provides an unprecedented opportunity to potentiate the innate immune response of natural killer cells toward target tumor cells through thermally triggered cell-specific desialylation, which paves the way for *in vivo* glycoimmune-checkpoint-targeted cancer therapeutic intervention.

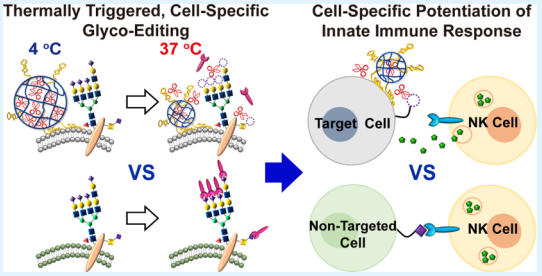

KEYWORDS: *aptamer, cell-specific, glyco-editing, lectin recognition, microgel, thermally triggered*

INTRODUCTION

Cell surface glycans are the key components that mediate ligand−receptor recognition, cell−cell communications, intracellular signaling and so forth in a variety of physiological and pathological processes.[1,2] Thus, editing of cell surface glycan chains (*i.e.*, glyco-editing), including the trimming, transformation, and addition of carbohydrates, allows for elaborate modulation of cell functions and interactions,[3,4] which fosters the deep understanding of the relationship between glycan structures and biological effects. For example, Engle et al. reconstituted glycan sialyl-Lewis^a in mice using genetic engineering and revealed the role of this glycan antigen in pancreatic disease pathogenesis.[3] More importantly, considering the roles glycans play in immune evasion,[5] just as in the case of sialylated glycans on tumor cells for inhibiting the activation of natural killer (NK) cells through engagement with sialic acid-binding Ig-like lectins (Siglec) receptors,[6−9] glyco-editing brings breakthroughs to cancer therapy by breaking glyco-immune checkpoint axis to relieve immunosuppression.[10]

To manually edit cell surface glycans, the widely used approaches are genetic engineering,[3,11] metabolic oligosaccharide engineering (MOE),[12−16] and chemoenzymatic methods.[4,17−21] Despite much progress, these methods suffer from one or more drawbacks: (1) complicated technical requirements (especially for manipulation of glycosyltransferase gene expression);[22] (2) stretched time course (*e.g.*, for MOE, 24−72 h is needed);[15,16] (3) ill-defined editing specificity and limited editing efficiency; (4) potential detrimental effects, both of which are common problems for methods depending on cellular activities or endogenous functions;[21,23−25] and (5) lack of selectivity over cell types. These issues have plagued the *in situ* revelation of glycan recognition properties and hampered the application of glyco-editing in complicated bona fide biosystems. In particular, when deploying glyco-editing platforms in the scenario of cancer-immune intervention, side effects from glyco-editing on nontumor tissues during editing motif delivery stage should be avoided. Thus, development of *in situ*, cell-specific glyco-editing tools while exempting the dependence on cellular "internal" pathways is in urgent need.[21]

Received: August 24, 2020
Accepted: November 17, 2020
Published: November 25, 2020

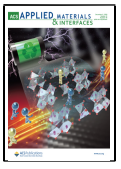

https://dx.doi.org/10.1021/acsami.0c15212
ACS Appl. Mater. Interfaces 2020, 12, 54387−54398

Scheme 1. Principle of Thermally Triggered, Cell-Specific Enzymatic Glyco-Editing; Schematic Illustration for Preparation of Neu@MG@Apt (a); Schemes Showing Neu@MG@Apt-Based Sia Trimming for Cell-Specific Regulation of Lectin Recognition (b) and Potentiation of the Innate Immune Response (c)

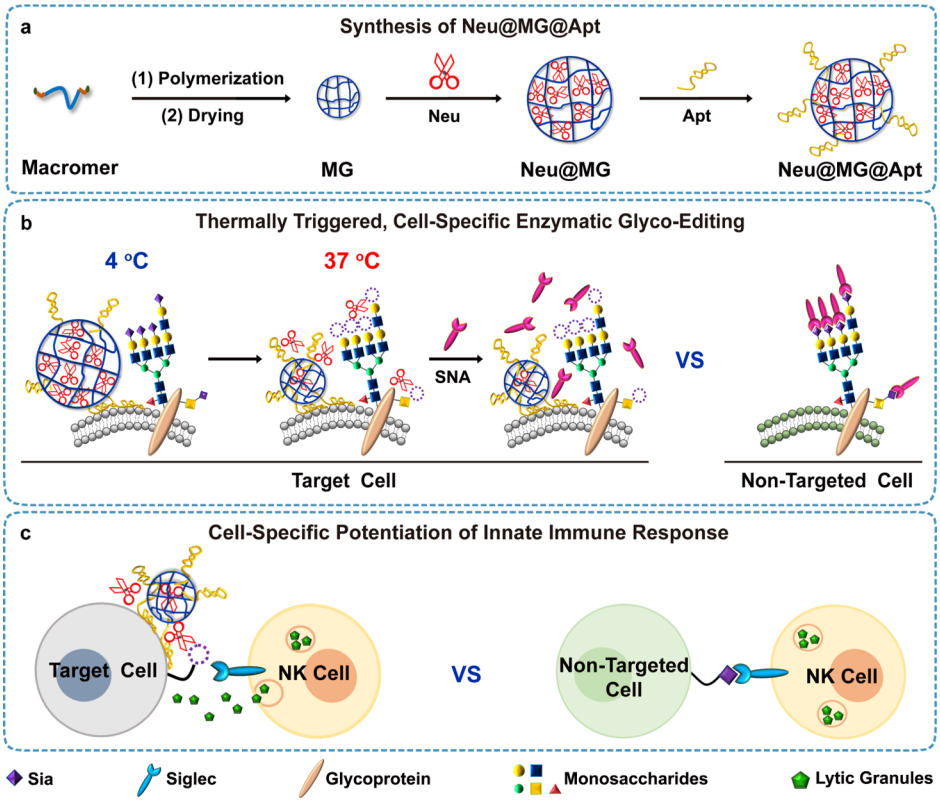

To meet the challenge, one needs to (1) directly edit cell surface glycans from the "*outside*" of cells and, in this regard, *in situ* glyco-editing using glyco-editing enzymes is a favorable choice, owing to the highly efficient and noninvasive features;[4,17−21,26,27] (2) localize the editing events to the cells of interest and, therefore, precision spatiotemporal control of enzyme activity is an undoubted necessity. During the preparation of the article, a glyco-editing enzyme lacking lectin domains was fused with an antibody for selectively stripping sialoglycans from breast cancer cells;[28] however, this method relies on the availability of specifically structured enzymes, and is therefore not a predictably effective strategy in general. Different from this, our solution is endowing glyco-editing enzymes with cell recognition capability and triggering the enzymes to function only after the enzymes reach the target cells. Owing to the high specificity and affinity toward cells, aptamers are desirable motifs for guiding enzymes to the target cells.[27,29] When it comes to switching on enzyme activity, it is beneficial to modulate the accessibility of enzymatic catalytic center rather than direct disturbing enzymatic activity.[30,31] This modulation can be implemented through encapsulation of enzymes, followed by stimuli-trigged release, with several types of stimuli as candidate triggers, including chemical (pH variation, chelating agents, bond-cleaving agents, *etc.*) and physical (light, temperature, *etc.*) handles.[27,32,33] We have encapsulated glyco-editing enzymes in a metal−organic framework and used EDTA to trigger enzyme release.[27] However, the cytotoxicity issue of EDTA (0.5 M) limits its application in authentic biosystems. In this context, temperature-based trigger offers an ideal solution in terms of easy operation and excellent biocompatibility.[34,35]

Herein, we develop a thermally triggered, cell-specific glyco-editing strategy for *in situ* regulation of cellular recognition and potentiation of the innate immune response on target cells. The achievement of precision spatiotemporal control of editing events relies on the orchestration of glycan remodeling capability of a glyco-editing enzyme and cell recognition specificity of an aptamer with a thermally sensitive intelligent microgel (MG) (Scheme 1). Sialic acid (Sia), a key monosaccharide building block that terminates glycan chains and participates many critical cellular processes,[36,37] is selected as the editing object, because of the promising prospect for modulating antitumor immunity.[7−9] α2-3,6,8,9 Neuraminidase A (Neu) with specific Sia cleavage capability[38] is thus utilized as the model glyco-editing enzyme. MDA-MB-231 cells, a triple negative, tumorigenic human breast epithelial cell line, are chosen as the target cells, and correspondingly, an aptamer with high affinity toward MDA-MB-231 cells, LXL-1-A (abbreviated as Apt),[39] is used to direct the enzyme to the target cells. Neu can be encapsulated into MG by swelling at 4 °C, followed by assembly of Apt on the MG surface (Scheme 1a). The yielded probe can be specifically guided to the target cells by aptamer at 4 °C, with enzyme catalytic center blocked by the gel (inaccessible state); while upon increasing temperature to 37 °C, MG shrinkage occurs, leading to fast release of the encapsulated Neu (accessible state, Scheme 1b). Because of the slow diffusion rate of the enzyme and high effective local enzyme concentration,[27,40,41] the released Neu performed localized Sia trimming on the target cells, thus achieving cell-specific glyco-editing. This operation specifically alters the binding extent of the target cells toward a Sia-recognizing lectin, *Sambucus nigra* agglutinin (SNA), in both

https://dx.doi.org/10.1021/acsami.0c15212
ACS Appl. Mater. Interfaces 2020, 12, 54387−54398

single- and cocultured cell conditions (Scheme 1b). Owing to the exemption of the dependence on intracellular functions, tumor-specific glyco-editing is also achieved, for the first time, on tissue slices. We are also intrigued by the prospect of performing thermally triggered glyco-editing on a given type of tumor cells to boost the immune response. After executing cell-specific Sia trimming on cultured cells, enhanced killing activity is observed for NK cells toward target cells rather than nontargeted cells (Scheme 1c), underlining the opportunity of exploiting our method to potentiate innate antitumor immunity while avoiding perturbation of glycans on other cells.

EXPERIMENTAL SECTION

Synthesis of MG..[42,43] A total of 60 g of dry Pluronic F127 (F127), 4.1 g of L-lactide, and 90 mg of tin-2-ethylhexanoate were placed into a 500 mL flask under a N_2 atmosphere. The mixture was stirred at 200 °C for 2 h and 160 °C for 4 h and then cooled to room temperature. The obtained Pluronic F127-*co*-oligo(L-lactic acid) copolymer (F127-LA) was purified by the following steps three times: initial dissolution in dichloromethane, subsequent precipitation in anhydrous ether, and final centrifugation at 6000 rpm for 10 min. Then, the F127-LA was dried at 60 °C under vacuum for 1 day.

The as-prepared F127-LA (30 g) was dissolved in 300 mL of dichloromethane in a 500 mL flask and cooled to 0 °C in an ice bath. Then, 1.31 mL of triethylamine and 1.58 mL of acryloyl chloride were added to the flask, and the mixture was stirred for 12 h at 0 °C and 12 h at room temperature. After filtering the mixture, Pluronic F127-*co*-oligo (L-lactic acid) diacrylate macromer (F127-LA-DA) was obtained by pouring the filtrate into a large excess of anhydrous ether. The product was purified by the following steps three times: initial dissolution in dichloromethane, subsequent precipitation in hexane, and final centrifugation at 6000 rpm for 10 min. Finally, it was dried at 70 °C under vacuum for 1 day.

MG was prepared by inverse suspension polymerization in a N_2 atmosphere in a 250 mL four-neck flask fitted with a reflux condenser and a mechanical Teflon stirrer. Heptane (120 mL) and 4.2 g of Span 60, as the continuous phase, were added to the flask. After heating the flask to 70 °C using an oil bath, the freshly mixed dispersed phase, containing 5 mL of F127-LA-DA aqueous solution (14.7% w/w) with ammonium persulfate (APS) and ascorbic acid (AA) (3 wt % APS and 2.3 wt % AA of the macromer), was added dropwise at a rate of 1 drop/s into the flask. The reaction was allowed to proceed for 1 h at a stirring speed of 500 rpm. The resulting MG was separated from the solvent by centrifugation at 8000 rpm for 5 min and washed by the following steps three times: initial dissolution in acetone, subsequent precipitation in deionized water, and final filtration. After being dried at 4 °C, the MG was preserved in a desiccator at 4 °C.

Preparation of Neu@MG and Neu@MG@Apt. To load Neu into MG, 15 mg of dried MG was added to 2 mL of PBS containing Neu of 200 U/mL, and the mixture was stirred at 800 rpm for 72 h at 4 °C. The Neu@MG was separated by centrifugation at 8000 rpm for 3 min at 4 °C and washed with 5 mL of PBS at 4 °C five times to remove the proteins adsorbed on the surface of MG.

To assemble Apt on Neu@MG, 10 μL of 100 μM TR-Apt was added to 100 μL of PBS containing Neu@MG of 40 U/mL in equivalent Neu unit. The mixture was incubated at 4 °C on a constant temperature mixer with a speed of 800 rpm for 4 h. The product Neu@MG@Apt was collected by centrifugation at 10,000 rpm for 10 min at 4 °C, washed with PBS three times, redispersed in 100 μL of PBS, and then stored at 4 °C. The Neu@MG@Apt in aqueous solution at 4 °C was characterized by confocal laser scanning microscopy (CLSM), and the Neu@MG@Apt after drying at 37 °C for 2 h was characterized by scanning electron microscopy (SEM).

Analysis of the Neu Loading Efficiency. The amount of Neu encapsulated in Neu@MG was determined using the Micro BCA Protein Assay Kit. The Neu loading efficiency was calculated by dividing the Neu amount with the total Neu amount added for probe preparation.

Demonstration of Temperature-Sensitive Particle Size Change for MG, Neu@MG, and Neu@MG@Apt. A batch of centrifuge tubes were prepared by adding 10 μL of MG (or Neu@MG or Neu@MG@Apt) and 3 mL of H_2O to each tube in a thermostat water bath of 4 °C. Then, the temperature was gradually increased by maintaining at each temperature point (4, 10, 15, 20, 25, 27, 29, 31, 33, 35, 37, 39, 41, 45, 50 °C) for 30 min. At the end of each period, three tubes were taken out and subjected to dynamic light scattering (DLS) analysis.

Analysis of Released Neu Concentration from Neu@MG and Neu@MG@Apt with Increasing Temperature. A batch of centrifuge tubes were prepared at 4 °C by adding 210 μL of MG (0.05 mg/mL) or Neu@MG or Neu@MG@Apt (28 μg/mL in equivalent Neu concentration) to each tube. Then, the tubes were incubated at different temperatures (4, 10, 15, 20, 25, 27, 29, 31, 33, 35, 37, 39, 41, 45, 50 °C) for 30 min with three tubes for each temperature. The supernatants were collected from tubes by centrifugation at 10,000 rpm for 1 min at 4 °C and measured by Micro BCA Protein Assay Kit. The absorbance value at 562 nm was recorded using a Varioskan Flash spectral scanning multimode reader.

Demonstration of Blocked Neu Accessibility in Neu@MG and Neu@MG@Apt at 4 °C. To each well on 96-well plates, 100 μL of Neu, Neu@MG, or Neu@MG@Apt (40 U/mL in equivalent Neu unit) and 0.05 mg/mL MG in PBS were added and mixed with 100 μL of working solution from Amplex Red Neuraminidase (Sialidase) Assay Kit. After incubation of the plates at 4 and 37 °C for 1 h, the 562 nm absorbance was recorded using the spectral scanning multimode reader.

Analysis of Catalytic Activity of Released Neu from Neu@MG and Neu@MG@Apt with Time Extension. A batch of centrifuge tubes were prepared at 4 °C by adding 210 μL of MG (0.05 mg/mL) or Neu@MG or Neu@MG@Apt (28 μg/mL in equivalent Neu concentration) to each tube. Then, the tubes were incubated at 37 °C for different periods of time (1, 2, 3, 4, 5, 6, 7, 8, 9, 10, 11, 12, 13, 14, 15, 20 and 30 min) with three tubes for each period. After centrifugation at 10,000 rpm for 1 min at 4 °C, the supernatants were collected and subjected to incubation with 100 μL of the working solution from Amplex Red Neuraminidase (Sialidase) Assay Kit at 37 °C for 1 h. Then, the 562 nm absorbance was recorded using the spectral scanning multimode reader.

Thermally Triggered Non-Cell-Specific Sia Trimming. MDA-MB-231 (or MCF-7) cells were seeded on four-well confocal dishes and cultured in a 5% CO_2 incubator at 37 °C for 12 h. After discarding the culture medium, the cells were blocked with PBS containing 10% goat serum at 37 °C for 30 min and washed with PBS three times. Then, the cells were, respectively, incubated with Neu (0.5 U/mL) or Neu@MG (0.5 U/mL in equivalent Neu unit) at 4 or 37 °C for 30 min. As a control, cells without treatment were incubated in PBS at 37 °C for 30 min. After washing with PBS three times, the cells were allowed to incubate with 100 μL of Fluorescein isothiocyanate-labeled SNA (SNA-FITC) (0.02 mg/mL) at 4 °C for 30 min. After washing with PBS, the cells were immediately imaged by CLSM.

Verification of Cell-Specific Recognition of Neu@MG@Apt. MDA-MB-231 (Apt binding +) and MCF-7 cells (Apt binding −) were separately seeded, blocked, and washed. Then, the cells were allowed to incubate in 100 μL of PBS containing TR-Apt (1 μM), TR-Ran (1 μM), Neu@MG@TR-Apt (0.5 U/mL in equivalent Neu unit), and Neu@MG@TR-Ran (0.5 U/mL in equivalent Neu unit) at 4 °C for 30 min. After washing with PBS, the fluorescence of TR on the cell surface was imaged with CLSM. The emission signal from 605 to 685 nm was collected under 594 nm excitation.

Thermally Triggered Cell-Specific Sia Trimming by Neu@MG@Apt. After seeding, blocking, and washing, MDA-MB-231 or MCF-7 cells were subjected to 1st-incubation with Neu@MG@Apt solution of 0.5 U/mL (in equivalent Neu unit) at 4 °C for 30 min. After washing three times with PBS, the cells were subjected to 2nd-incubation at 4 or 37 °C for 30 min. After washing with PBS three times, the cells were subjected to SNA-FITC incubation and CLSM imaging.

https://dx.doi.org/10.1021/acsami.0c15212
ACS Appl. Mater. Interfaces 2020, 12, 54387−54398

Demonstration of Sia Trimming Specificity of Neu@MG@Apt. After seeding, blocking, and washing, MDA-MB-231 cells were subjected to incubation with Neu@MG@Apt of 0.5 U/mL (in equivalent Neu unit) at 4 °C for 30 min. After washing three times with PBS, the cells were allowed to incubate in 100 μL of PBS containing poly-2,8-*N*-acetylneuraminic acid sodium salt (PSia) of 20 mg/mL at 37 °C for 30 min. After washing with PBS three times, the cells were subjected to SNA-FITC incubation and CLSM imaging.

Cell-Specific Regulation of Lectin Binding in Cocultured Cell Setting. After trypsin digestion and centrifugation, MDA-MB-231 and MCF-7 cells were separately incubated in RPMI-1640 medium. The cell number was determined using a Countess II FL Automated Cell Counter. Then, the two types of cell suspensions were mixed with a cell concentration ratio of 1:1. The mixed cell suspension was seeded at a density of 4×10^5 cells/mL and cocultured in RPMI-1640 medium for 12 h. After blocking and washing, the wells were divided into four groups. Group 1 (control group): The cells were incubated in PBS at 37 °C for 30 min. Group 2: The cells were incubated in 0.5 U/mL Neu at 37 °C for 30 min. Group 3: The cells were incubated in Neu@MG solution of 0.5 U/mL (in equivalent Neu unit) at 37 °C for 30 min. Group 4: The cells were subjected to 1st-incubation with Neu@MG@Apt solution of 0.5 U/mL (in equivalent Neu unit) at 4 °C for 30 min. After washing three times with PBS, the cells were subjected to 2nd-incubation at 37 °C for 30 min. After washing with PBS three times, the cells from all groups were subjected to SNA-FITC incubation. The cells in groups 1 and 2 were further incubated with TR-Apt at 4 °C for 30 min for identification of target MDA-MB-231 cells. Then, cells were carefully washed and imaged with CLSM. The emission signals were collected from 515 to 564 nm and from 605 to 685 nm under 495 nm and 594 nm excitation, respectively.

To validate the CLSM results by flow cytometry, MDA-MB-231 cells were prestained using 5 μM DiD at 4 °C for 10 min. The cell seeding, coculturing and probe treatment procedures were performed as described above. Then, the cells were subjected to incubation with 0.04 mg/mL SNA-FITC at 4 °C for 1 h. After washing with PBS two times, the cells were measured by Attune NxT Acoustic Focusing Cytometer using BL-1 and RL-1 channels.

Tumor-Specific Glyco-Editing on Tissue Slices. Six female BALB/c nude mice, four- to six-week-old, 18−20 g in weight, were purchased from KeyGen Biotech Co., Ltd. (China). All animal experiments were preformed according to the Institutional Animal Care and Use Regulations (no. IACUC-003-3) approved by Experimental Animal Ethics Committee of KeyGen Biotech Co., Ltd. (China). A mouse MDA-MB-231 tumor xenograft model was established by subcutaneous injection of MDA-MB-231 cells (1×10^6) into the selected positions of nude mice. When the volume of the subcutaneous tumor reached 100 cm^3, the mice were sacrificed, and the subcutaneous tumors with marginal normal tissues and the normal breast tissues were both harvested. After performing standard fixing operation, the tissue samples were embedded in histological paraffin and cut into 4 μm-thick slices. Three types of slices were obtained: tumor tissue slices, tumor edge tissue slices, and normal tissue slices. The slices were stained with hematoxylin−eosin (H&E) through standard steps.

After dewaxing in xylene for 2 h, the tissue slices were sequentially hydrated in ethanol baths of decreasing concentrations (100, 95, 90, 80, 75, 70, and 50%) for 3 min/bath. After being immersed in H_2O three times (3 min each), the tissue slices were blocked with 5% bovine serum albumin (BSA) at 37 °C for 1 h and washed three times by PBS immersion (3 min each). Then, the tissue slices were subjected to incubation with Neu@MG@Apt or PBS at 4 °C for 1 h, followed by three-time washing with PBS (5 min each) and incubation at 37 °C for 2 h. After washing three times with PBS for 5 min each, the tissue slices were incubated with 0.04 mg/mL SNA-FITC at 4 °C for 5 h. Then, the tissue slices were washed with PBS three times (5 min each) and stained with DAPI at room temperature for 20 min, followed by PBS washing three times (5 min each). Then, the tissue slices were dehydrated in ethanol baths of increasing concentrations (50, 70, 80, 90, 95, and 100%) for 3 min/bath, transferred to xylene, and further immersed for 12 min to make the tissue slices transparent. Finally, the tissue slices were sealed with neutral resin and imaged with CLSM. The emission signals were collected from 415 to 500 nm and 515 to 564 nm under 405 nm and 495 nm excitation, respectively.

For tumor edge tissue slices, anti-integrin $\alpha_v\beta_3$ antibody was used to indicate tumor cells. Thus, the experimental procedure was similar to that for tumor/normal tissue slices except for two additional operations: (1) before blocking with BSA, the slices were hydrated in Improved Citrate Antigen Retrieval Solution bath at 95 °C for 10 min, followed by immersion in H_2O_2 three times (3 min each); (2) before SNA-FITC staining, the tissue slices, after being washed three times with PBS for 5 min each, were incubated with 1 μg/mL integrin $\alpha_v\beta_3$ (23C6) at 4 °C for 10 h, followed by washing three times with PBS for 5 min each and incubation with Goat Polyclonal Secondary Antibody to Mouse IgG-H&L (Alexa Fluor 647) with a dilution ratio of 1:1000, at 37 °C for 1 h. Finally, for CLSM imaging of antibody staining, the emission signals were collected from 680 to 730 nm under excitation at 647 nm.

Demonstration of Cell-Specific Potentiation of NK Cell Cytotoxicity with CCK-8 Assay. MDA-MB-231 (or MCF-7) cells in RPMI-1640 medium (100 μL) were pipetted into the wells of a 96-well plate with a cell density of ∼10,000 cells per well. The plate was then incubated at 37 °C for 24 h in 5% CO_2 atmosphere. After removal of the medium, the cells were divided into eight groups. Groups 1 and 5: incubation in PBS at 4 °C for 30 min and then 37 °C for 30 min; groups 2 and 6: incubation with Neu (0.5 U/mL, 100 μL per well) at 37 °C for 30 min; groups 3 and 7: incubation with Neu@MG (0.5 U/mL in equivalent Neu unit, 100 μL per well) at 37 °C for 30 min; groups 4 and 8: incubation with Neu@MG@Apt (0.5 U/mL in equivalent Neu unit, 100 μL per well) at 4 °C for 30 min, followed by three-time washing with PBS, and incubation at 37 °C for 30 min. After washing with PBS three times, all the groups were subjected to trypsin treatment followed by removal of the trypsin. It should be noted that the purpose of trypsin treatment is to ensure a similar NK-tumor cell contact condition for single- and cocultured cell settings (*vide infra*), considering a 20-fold higher cell seeding density in single-cultured cell setting compared with that in cocultured cell setting. Then, to each well of groups 5−8 and 1−4, 100 μL of the RPMI-1640 medium with and without 10,000 NK cells was added, respectively, and the plate was incubated at 37 °C for 8 h. After removal of the medium and washing with PBS three times, 100 μL of the RPMI-1640 medium containing 10 μL of CCK-8 reagent was added to each well, and the plate was incubated at 37 °C for 4 h. Then, the absorbance at 450 nm was recorded using the spectral scanning multimode reader.

Demonstration of Cell-Specific Potentiation of NK Cell Cytotoxicity in Cocultured Cell Setting. MDA-MB-231 and MCF-7 cells were each seeded at a density of 2×10^5 cells/mL and cocultured in RPMI-1640 medium for 12 h. After blocking and washing, the dishes were divided to the same eight groups as in the above NK cell cytotoxicity analysis by the CCK-8 assay. After incubation with different probes or PBS, 100 μL of the RPMI-1640 medium with and without 4×10^5 NK cells was, respectively, added to wells in groups 5−8 and 1−4 and incubated at 37 °C for 8 h. After washing with PBS three times, 100 μL of 2 μM calcein-AM reagent was added to each well and incubated at 37 °C for 30 min. Then, the cells in groups 1−3 and 5−7 were further incubated with TR-Apt at 4 °C for 30 min for identification of target MDA-MB-231 cells. The cells were then carefully washed and imaged with CLSM. The emission signals were collected from 500 to 540 nm and 605 to 685 nm under 488 nm and 594 nm excitation, respectively. The CLSM results were also validated by flow cytometry using DiD staining to indicate MDA-MB-231 cells.

Statistical Analysis. All data were representative results from at least three independent experiments and average ± standard deviation were shown. Statistical analysis was performed using unpaired two-tailed Student's *t*-test unless noted otherwise. $*p < 0.05$, $**p < 0.005$, $***p < 0.0005$ were considered statistically significant, and $p \geq 0.05$ was considered statistically not significant (NS).

https://dx.doi.org/10.1021/acsami.0c15212
ACS Appl. Mater. Interfaces 2020, 12, 54387−54398

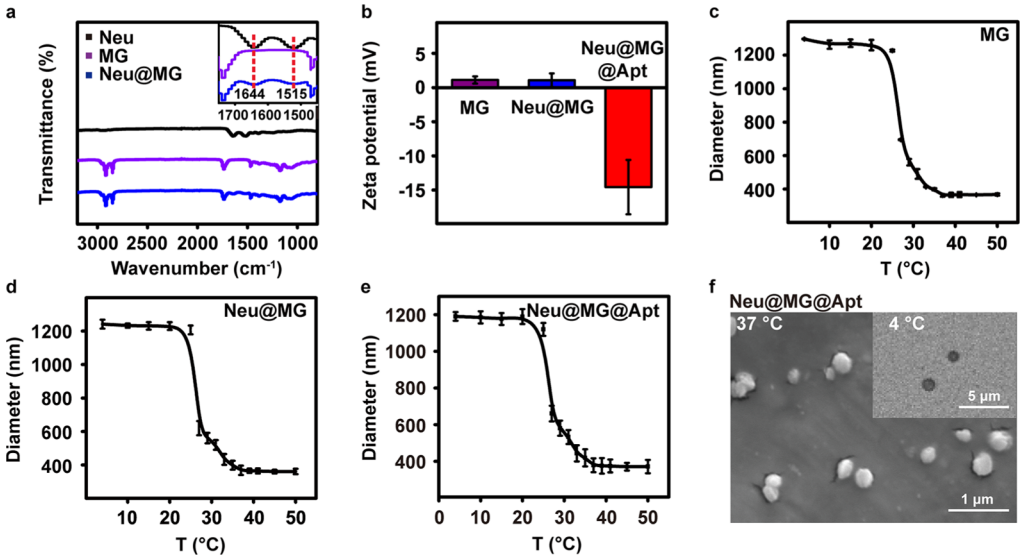

Figure 1. Characterization of Neu@MG@Apt. (a) FTIR spectra of Neu, MG, and Neu@MG. Inset in (a): magnified figure for the region between 1500-1700 cm^{-1}. (b) Zeta potentials of MG, Neu@MG, and Neu@MG@Apt. Mean ± s.d. of three independent experiments are presented. Particle size analysis of MG (c), Neu@MG (d) and Neu@MG@Apt (e) with increasing temperature by DLS. Mean ± s.d. of three independent experiments are presented. (f) SEM image and optical micrograph (inset) of Neu@MG@Apt after drying at 37 °C and dispersing in PBS at 4 °C, respectively.

RESULTS AND DISCUSSION

Synthesis and Characterization of Neu@MG@Apt. To implement controllable enzyme encapsulation and release while minimizing influence on enzyme activity, a biocompatible, negatively thermally sensitive MG is chosen and prepared by inverse suspension polymerization from a macromer, Pluronic F127-*co*-oligo(L-lactic acid) diacrylate (F127-LA-DA, Figure S1), according to a literature with slight modifications.[42,43] Owing to the swelling property of MG at 4 °C, direct mixing dried MG (15 mg) with Neu (279 μg) in PBS leads to facile loading of Neu into MG, yielding Neu@MG with a loading efficiency of 70%, which is obtained by dividing the encapsulated amount of Neu, determined by bicinchoninic acid (BCA) assay, with the total amount of Neu added. The successful encapsulation is confirmed by Fourier transform infrared spectroscopy (FTIR) characterization of Neu@MG after extensive washing. The peaks at 1644 and 1515 cm^{-1} can be, respectively, attributed to C═O stretching and N−H bending vibrations of the protein (Figure 1a).[42] To endow cell binding specificity to Neu@MG, Apt, with Texas Red (TR) labeled at the 5′-end to indicate cell binding, is incorporated by adsorption on Neu@MG to form the final probe, Neu@MG@Apt. This assembly step leads to a variation of Zeta potential from 1 to −15 mV (Figure 1b).

With the probe successfully prepared, the thermally responsive modulation of Neu release (accessibility) is systematically evaluated. We first investigate the volume change of MG, Neu@MG and Neu@MG@Apt upon temperature increasing from 4 to 50 °C by DLS. The MG is swollen at 4 °C, and exhibits a substantial decrease of diameter at temperature higher than 27 °C (Figure 1c), which is the volume phase transition temperature (VPTT). The plateau diameter, obtained at 37 °C, is about one-third of the average diameter at 4 °C. The Neu@MG (Figure 1d) and Neu@MG@Apt (Figure 1e) display trends similar to those of MG. The morphology of Neu@MG@Apt at 4 and 37 °C is observed by optical microscopy and SEM. The probe shows a diameter of 0.95−1.32 μm with a spherical morphology at 4 °C (Figure 1f, inset), while after drying at 37 °C for 2 h, the diameter decreases to 220−334 nm (Figure 1f).

Demonstration of Thermally Triggered Modulation of Neu Accessibility. The thermally triggered, protein release concentration from Neu@MG (Figure 2a) and Neu@MG@Apt (Figure 2b) along with increasing temperature is monitored. After incubation of probes at each temperature for 30 min followed by centrifugation, the supernatants are collected and subjected to BCA protein quantification assay. At temperature below VPTT, both types of probes release negligible amount of protein, suggesting excellent encapsulation of Neu by MG. Whereas at temperature higher than VPTT, a significant protein release is observed with a maximal release percentage, 70% for Neu@MG and 68% for Neu@MG@Apt of the encapsulated amount, obtained at 37 °C. The influence of MG after incubation at different temperatures for 30 min on protein quantification can be ignored as evidenced by the indiscernible protein signal (Figure S2a).

The blocking of Neu activity by MG during probe delivery stage is a precondition for minimizing non-specific editing. Thus, we use Amplex Red Neuraminidase (Sialidase) Assay Kit with fetuin as the enzymatic substrate to evaluate the Neu activity of the probes by direct incubation of probes with the working solution of the Kit. The influence from MG on Neu activity analysis is first excluded (Figures 2c and S2b). Both Neu@MG and Neu@MG@Apt exhibit indiscernible Sia cleavage activity at 4 °C, while free Neu of the encapsulated amount displays an obvious cleavage activity at this temperature (72% of that at 37 °C, Figures 2c and S3), suggesting efficient blocking of Neu accessibility and thus activity by MG at 4 °C. However, after incubation at 37 °C for 1 h, these probes display substantial catalytic activities, which are 61% for Neu@MG and 57% for Neu@MG@Apt of that for free Neu of the encapsulated amount (Figure 2c). The agreement of these data with the protein release percentages obtained by BCA assay (Figure 2a,b) provides proof for the largely unaffected

https://dx.doi.org/10.1021/acsami.0c15212
ACS Appl. Mater. Interfaces 2020, 12, 54387−54398

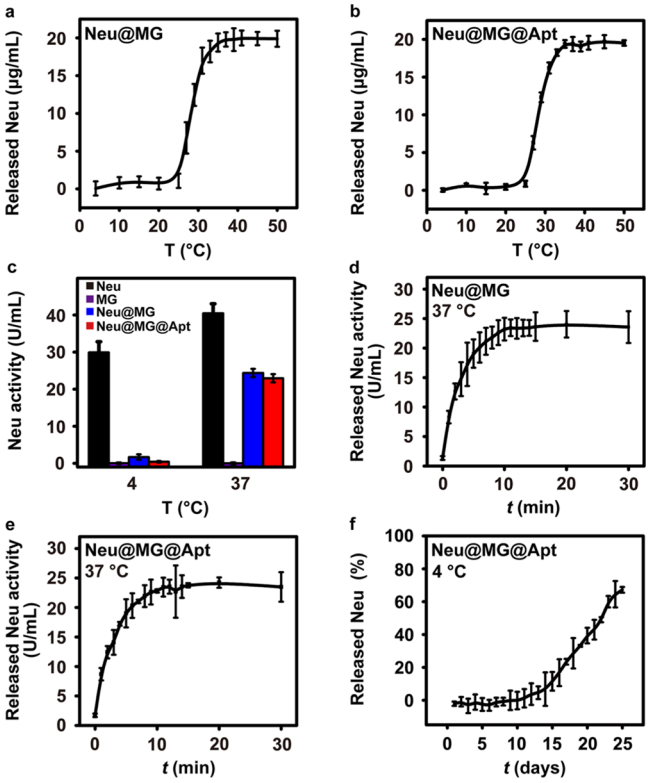

Figure 2. Demonstration of the thermally triggered release of Neu for modulation of enzymatic accessibility. Concentration of released Neu from Neu@MG (a) and Neu@MG@Apt (b) after incubation at different temperatures for 30 min. (c) Neu inaccessibility at 4 °C but accessibility at 37 °C in Neu@MG or Neu@MG@Apt as measured by enzyme activity analysis using free Neu of encapsulated amount as the control. The influence from MG on Neu activity analysis at different temperatures is excluded. Enzyme activity analysis of released Neu from Neu@MG (d) and Neu@MG@Apt (e) after incubation at 37 °C for different periods of time. (f) Demonstration of the stability of Neu@MG@Apt. Percentage of released Neu from Neu@MG@Apt of encapsulated amount after incubation at 4 °C for different periods of time. Mean ± s.d. of three independent experiments are presented.

Neu activity during enzyme encapsulation and release operations.

The time courses of Neu release at 37 °C from Neu@MG and Neu@MG@Apt are also tracked. To avoid continuous release of Neu during activity detection process, released Neu for each time period should be collected by centrifugation prior to measurement with the Kit. A fast release is observed for Neu@MG, with the arrival of 50% and full plateau activity value at 1.6 and 11 min, respectively (Figure 2d). The assembly of Apt does not affect Neu release kinetics (Figure 2e). The fast release of Neu ensures the efficiency of subsequent Sia trimming in live cell settings.

Evaluation of the Stability and Cytocompatibility of Neu@MG@Apt. With *in vitro* thermally triggered Neu release demonstrated, the feasibility of utilizing the probes on live cells is next assessed. The stability of Neu@MG@Apt in PBS at 4 °C is first examined by recording protein release percentage (Figure 2f); the Neu release is negligible in the initial 10 days. The subsequent gradual leaching out of Neu might be because of the degradation of MG by hydrolysis of labile ester bonds.[42] The excellent biocompatibility of different MG-based probes and intermediate species is evidenced by high cell viabilities (>92%) through CCK-8 assay using MDA-MB-231 and MCF-7 cells as the model (Figure S4).[42] The effects of the involved components, including Pluronic F127 (F127), Pluronic F127-*co*-oligo(L-lactic acid) copolymer (F127-LA), F127-LA-DA, and MG, on Neu activity are also examined on live cells. Fluorescein isothiocyanate-labeled SNA (SNA-FITC) is utilized to indicate the cell surface sialylation level.[44] Upon Neu treatment, similar degree of fluorescence decrease on the cell surface as a result of Sia trimming is observed by CLSM imaging, regardless of the addition of these components (Figure S5), thus excluding the influence.

Thermally Triggered Sia Trimming on Live Cells. Thermally triggered, *in situ* Sia trimming is then performed using Neu@MG on MDA-MB-231 and MCF-7 cells, and the effects of this operation on SNA-FITC binding are evaluated. The 4 °C-incubation of Neu@MG with either type of cells for 30 min does not affect SNA-FITC binding signal as compared with the control cells (Figure 3a,c–e), while incubation with free Neu at the same temperature leads to substantial cleavage of Sia as evidenced by the negligible SNA-FITC binding on cell surface (Figure 3b,c), suggesting effective blocking of Neu accessibility by MG in live cell settings. In contrast, treatment of cells with Neu@MG at 37 °C for 30 min dramatically reduces lectin binding extent, as reflected by the indiscernible fluorescence on the cell periphery (Figure 3d,e).

The cleavage extent is comparable to cells undergoing free Neu treatment at 37 °C (Figure 3b,c). Thus, the decrease of lectin binding for Neu@MG-treated cells at high temperature can be attributed to efficient cleavage of cell surface Sia by released Neu from Neu@MG upon thermal trigger. To further support this claim, the influence of temperature on enzymatic activity is excluded by the observation of only slightly decreased cleavage activity of Neu at 4 °C compared with that at 37 °C (Figures 2c and 3b,c).

Thermally Triggered, Cell-Specific Sia Trimming. Having verified thermally triggered Sia trimming on live cells, we then proceed to endow this operation with cell specificity by using Neu@MG@Apt. To this end, we first demonstrate the specific recognition of Neu@MG@Apt toward MDA-MB-231 cells by observation of bright cell periphery fluorescence from Apt (with TR labeled), using MCF-7 cells as the negative control (Figure S6).[39] The cell binding capability is lost on either the target or the control cells, when we displace Apt with a random sequence in the probe.

Then, we perform cell-specific Sia trimming using Neu@MG@Apt and assess the feasibility of specific regulation of lectin recognition on target cells (Figure 3f,g). To ensure precision spatiotemporal control of the editing event, the probe delivery (4 °C) and enzyme catalysis (37 °C) steps need to be stringently separated; thus, a two-step incubation operation (referred to hereafter as Neu@MG@Apt-based Sia trimming) is needed. After 1st-incubation of cells with Neu@MG@Apt at an optimal concentration of 0.5 U/mL for 30 min (Figure S7) at 4 °C for probe anchoring, the cells are washed to remove the unbound probe and subjected to 2nd-incubation at 37 °C for 30 min, followed by SNA-FITC incubation and CLSM imaging. To demonstrate the role of thermal triggering, a group of cells are administrated to 2nd-incubation at 4 °C for 30 min with other conditions unchanged. For these cells, a lectin binding signal is observed similar to that on the control cells, again suggesting the blocking effect of MG at low temperature. However, for cells undergoing 2nd-incubation at

https://dx.doi.org/10.1021/acsami.0c15212
ACS Appl. Mater. Interfaces 2020, 12, 54387−54398

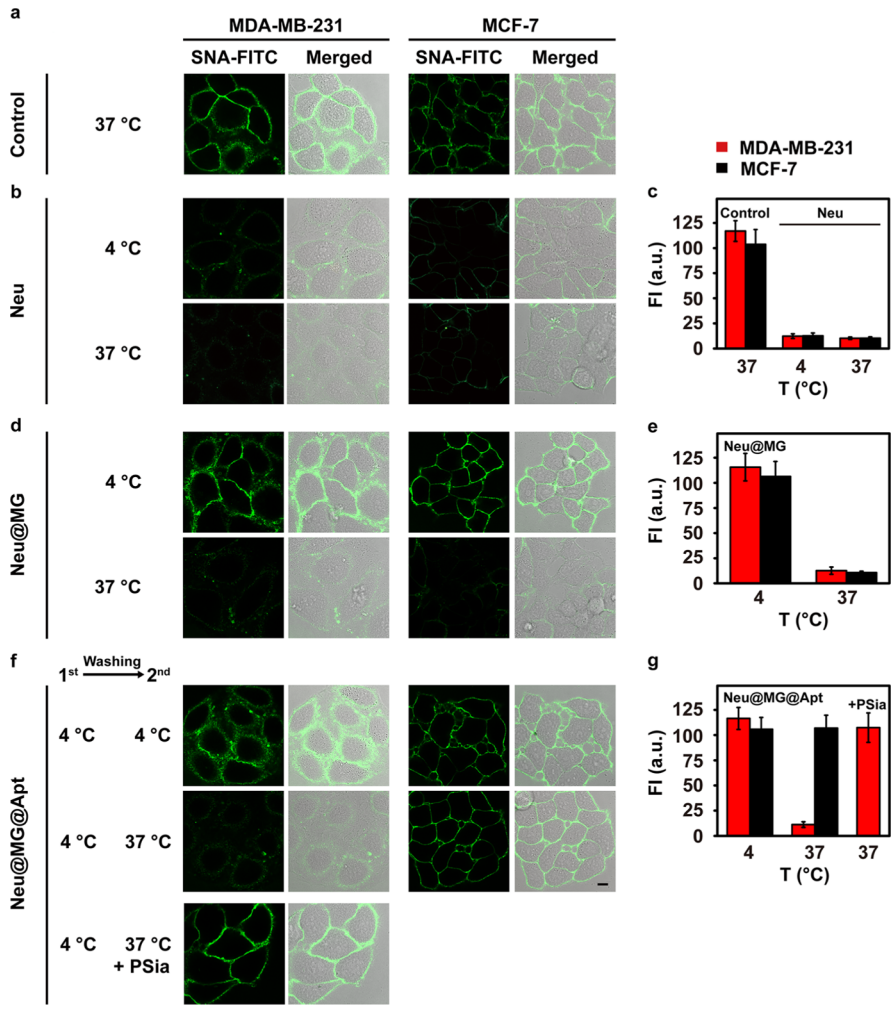

Figure 3. Demonstration of the effects of thermally triggered non-cell-specific and cell-specific Sia trimming on lectin recognition. (a) SNA-FITC staining of MDA-MB-231 and MCF-7 cells after incubation in PBS at 37 °C for 30 min. (b, d) SNA-FITC staining of MDA-MB-231 and MCF-7 cells after treatment with Neu (b) or Neu@MG (d) at 4 or 37 °C for 30 min. (f) SNA-FITC staining of MDA-MB-231 and MCF-7 cells after 1st-incubation with Neu@MG@Apt at 4 °C, washing, and subsequent 2nd-incubation at 4 or 37 °C. To demonstrate Sia trimming specificity, after 1st-incubation of cells with Neu@MG@Apt and subsequent washing, PSia is added during 2nd-incubation. Scale bar: 10 μm. (a,b,d,f) Representative results of three independent experiments. (c,e,g) Plots of SNA-FITC FI obtained from CLSM images at the periphery of MDA-MB-231 and MCF-7 cells from (a,b,d,f). Mean ± s.d. of three independent experiments are presented, measuring 10 cells each time.

37 °C, indiscernible lectin binding signal, indicating the occurrence of desialylation, can be observed only on MDA-MB-231 rather than MCF-7 cells (Figure 3f,g). This is because after the 1st-incubation and washing steps, only on MDA-MB-231 cells can the probe bind and then release Neu upon temperature trigger. These results demonstrate the necessity of Apt recognition for achievement of cell-specific glyco-editing. The released Neu during 2nd-incubation is estimated to be equivalent to 1.6×10^{-6} U per cell (Figure S8). An advantage of the proposed method is the short operation timeframe, which is about 90 min, much shorter than frequently used MOE-based glycan labeling methods (1−3 days).[15,16] The glyco-specificity of the method is validated by adding poly-2,8-*N*-acetylneuraminic acid (PSia) in the 2nd-incubation step, which leads to remarkably elevated lectin binding signal (Figure 3f,g) because of the competition between PSia and cell surface-linked sialylated glycans toward released Neu.

Cell-Specific Regulation of Lectin Binding in MDA-MB-231 and MCF-7 Cell Cocultured Setting. The cell specificity of the proposed method is further assessed in a more challenging experimental setting with MDA-MB-231 and MCF-7 cells cocultured. TR labeled on Apt, either additionally added or in Neu@MG@Apt, is used to indicate target MDA-MB-231 cells by red fluorescence. After performing *in situ* Neu@MG@Apt-based Sia trimming, only the cells with red staining, that is, MDA-MB-231 cells, display obvious decrease of green fluorescence from SNA-FITC binding, whereas MCF-7 cells show virtually unchanged lectin binding signals (Figure 4a, bottom, and Figure 4b). In contrast, treatment by free Neu or Neu@MG results in indiscriminate trimming of Sia on both types of cells, as reflected by the similar decrease extents of green fluorescence (Figure 4). The CLSM results are also manifested by flow cytometry (Figure S9). The achievement of cell-specific regulation of SNA-FITC binding here is due to the high effective local molarity of released enzyme as these high-molecular-weight protein species possess slow diffusion rates.[40,41] Although this cell specificity might gradually lose with stretched 2nd-incubation time, in our case, 30 min trimming time can ensure excellent cell specificity while efficient target-cell trimming as evidenced by the unaffected SNA-FITC fluorescence intensity (FI) on MCF-7 cells and almost disappearance of lectin binding on MDA-MB-231 cells

https://dx.doi.org/10.1021/acsami.0c15212
ACS Appl. Mater. Interfaces 2020, 12, 54387−54398

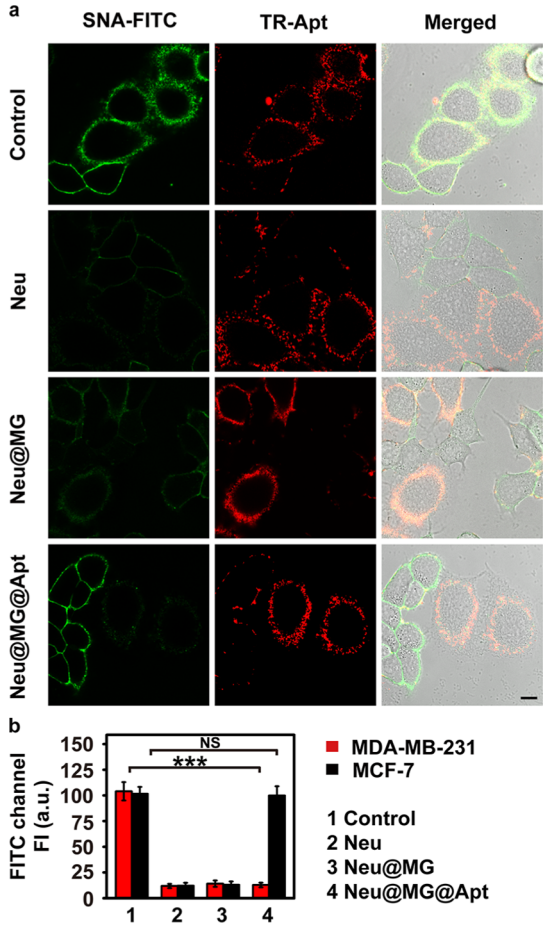

Figure 4. Cell-specific regulation of SNA-FITC binding in cocultured cell setting. (a) SNA-FITC staining of cocultured MDA-MB-231 and MCF-7 cells after Neu-, Neu@MG-, or Neu@MG@Apt-based Sia trimming. Cells without treatment are used as the control. Scale bar: 10 μm. (a) Representative results of three independent experiments. (b) FI of SNA-FITC at the periphery of MDA-MB-231 and MCF-7 cells from (a). Mean ± s.d. of three independent experiments are presented, measuring 10 cells each time. ***p < 0.0005 (p = 0.0000000054) (MDA-MB-231); NS, p = 0.57 (MCF-7).

(Figure 4b). A weak binding of the probe on MCF-7 cells can be also observed, which likely resulted from slightly compromised Apt binding specificity in complex cocultured cellular environment (Figure 4a, bottom); however, the low local Neu concentration is incompetent to exert effective trimming activity, again reflected by the negligible change of FITC fluorescence on MCF-7 cells compared to that on control cells (Figure 4b).

Tumor-Specific Glyco-Editing on Tissue Slices. The application expansion of glyco-editing technique from live cells to more authentic biosystems, such as tissue slices, is always considered an unsolved task because of the dependence on cellular endogenous functions of most glyco-editing strategies. Thus, the cell-function-independent editing feature of our method motivates us to perform tumor-specific glyco-editing on tissue slices. To this end, tumor and normal tissue slices are collected from paraffin-embedded tissue sections from MDA-MB-231 subcutaneous tumor xenografts and normal breast, respectively, in BALB/c nude mice. The histological differences between tumor and normal tissue slices are confirmed by hematoxylin and eosin (H&E) staining (Figure S10a, right) and a marked SNA-FITC binding to tumor tissues compared with normal tissues can be observed, because of the overexpression of Sia on the tumor cell surface.[36,37] Then, we perform thermally triggered Neu@MG@Apt-based Sia trimming on the two types of tissue slices. The tumor tissue slices display an obviously lower binding of SNA-FITC after glyco-editing, as reflected by weaker green fluorescence, compared with tumor tissue slices without editing (Figure S10a, top, and Figure S10b), which can be largely attributed to the Sia trimming on MDA-MB-231 cells by Neu@MG@Apt treatment. While on normal tissue slices, there are indiscernible change of lectin binding after editing operation (Figure S10a, bottom, and Figure S10c). The tumor-specific desialylation is also demonstrated on slices from the edge of the tumor tissues (Figure 5). Using anti-integrin $\alpha_v\beta_3$ antibody to indicate tumor tissues,[45] after Neu@MG@Apt-based Sia trimming, the regions with bright antibody binding signal (*i.e.*, tumor cells) display a substantially decreased binding of SNA-FITC. To further verify the cell specificity of Sia trimming by our method, tissue slices from bladder tumor are also collected, which display high Sia expression but should not be desialylated. After performing Neu@MG@Apt-based Sia trimming, negligible change of the SNA-FITC signal can be observed because of the incompetent binding of Neu@MG@Apt toward bladder tumor tissues (Figure S11). These data suggest the realization of tumor-specific glyco-editing on bona fide tissue slices for the first time, which represents an important step in the field of glyco-editing.

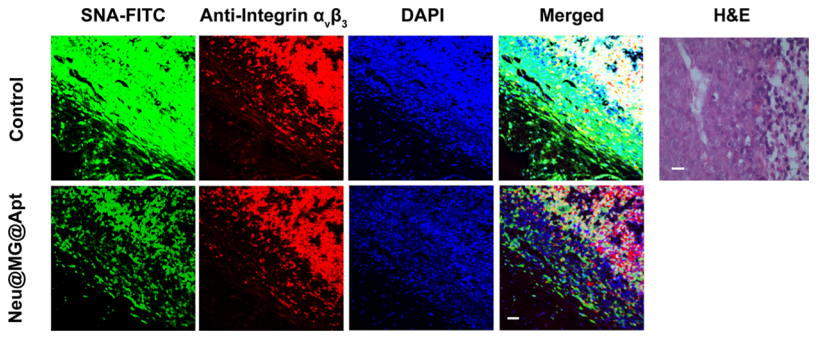

Figure 5. Glyco-editing on tumor edge tissue slices from subcutaneous MDA-MB-231 xenograft. SNA-FITC staining of tumor edge slices with and without Neu@MG@Apt-based Sia trimming treatment. Anti-integrin $\alpha_v\beta_3$ antibody staining indicates tumor tissues. The histological photomicrograph for the tumor edge slices is also shown. Scale bars: 50 μm. The images are representative results from ≥3 slices per section, n = 6 mice.

https://dx.doi.org/10.1021/acsami.0c15212
ACS Appl. Mater. Interfaces 2020, 12, 54387−54398

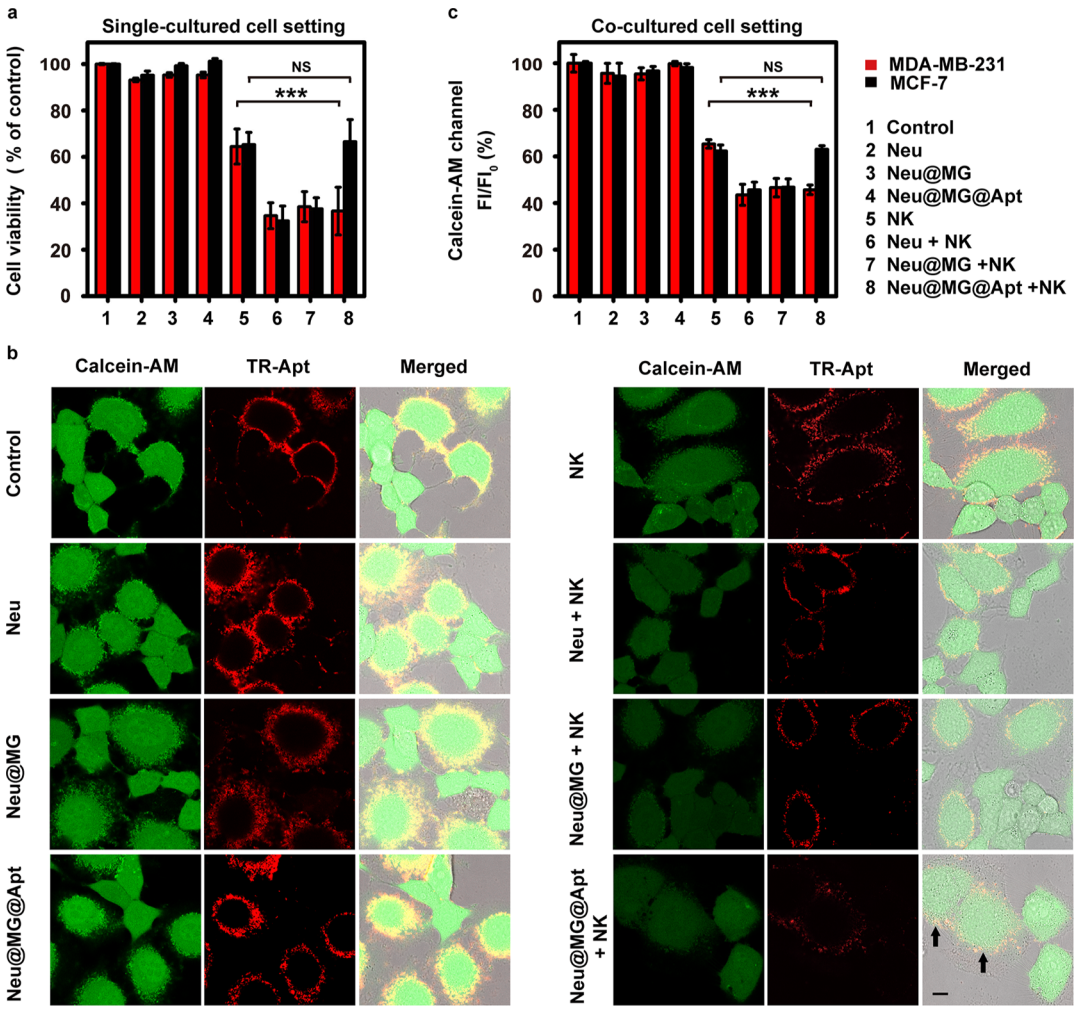

Figure 6. Cell-specific potentiation of NK cell killing activity by exerting Neu@MG@Apt-based Sia trimming in single- and cocultured cell setting. (a) Cell viability of separately cultured MDA-MB-231 and MCF-7 cells after PBS incubation, Neu treatment, Neu@MG treatment, or Neu@MG@Apt-based Sia trimming with and without combination of NK cell incubation, assessed by CCK-8 assay. Cytotoxicity is evaluated at a 1:1 effector/target (E/T) ratio. Mean ± s.d. of three independent experiments are presented. $^{**}p$ = 0.0027 (MDA-MB-231); NS, p = 0.79 (MCF-7). (b) CLSM images of cocultured MDA-MB-231 and MCF-7 cells after PBS incubation, Neu treatment, Neu@MG treatment, or Neu@MG@Apt-based Sia trimming with and without combination of NK cell incubation (1:1 E/T ratio). Cells with arrow indicated are target MDA-MB-231 cells. Scale bar: 10 μm. Images are representative of three independent experiments. (c) Plot of normalized Calcein-AM fluorescence intensity (FI/FI_0) at the periphery of MDA-MB-231 and MCF-7 cells from (b). FI, fluorescence intensity obtained from CLSM images; FI_0, fluorescence intensity on control cells. Mean ± s.d. of three independent experiments are presented, measuring 10 cells each time. $^{***}p < 0.0005$ (p = 0.000024) (MDA-MB-231); NS, p = 0.29 (MCF-7).

Potentiation of Innate Immune Response toward Target Cells. The achievement of cell-specific regulation of lectin binding by our method provides an unprecedented opportunity for precision modulation of the immune response toward live cells. It is well known that Sia is overexpressed in many tumor types[36,37] and exploited by tumor cells for inhibition of NK cell activation *via* the engagement of sialic acid-binding immunoglobulin-like lectin 7 (Siglec-7).[6] Thus, targeting the Sia−Siglec axis (glyco-immune checkpoint), either by cleaving Sia on tumor cells or blocking Sia−Siglec interactions, is a promising therapeutic strategy,[9,10] which has been carried out in preclinical models.[7,8] Among them, neuraminidase treatment of cancer cells, capable of removing the Siglec ligands, represents an easier way to enhance NK cell killing.[7,8] However, its *in vivo* feasibility remains to be ambiguous because of the concern regarding the side effects from desialylation during probe delivery stage.[7] Thus, to push forward Sia-Siglec-axis-targeted cancer immunological therapeutic intervention, we exploit our method to promote the immune response on a given type of cultured tumor cells. NK cells are purified from peripheral blood mononuclear cells (PBMCs), that are separated from peripheral blood of healthy people, and verified by flow cytometry (Figure S12).[46] The incubation of NK cells with separately cultured MDA-MB-231 and MCF-7 cells for 8 h leads to a cytolysis ratio of 65% and 64%, respectively, as measured by CCK-8 assay (Figure 6a). Longer NK cell incubation time renders a further higher cytotoxicity (Figure S13). The comparable cytolysis between the two cell types has also been reported by previous studies,[47−49] which might be related to the complicated interactions between tumor cell surface ligands with the activating and inhibitory receptors on NK cells.[50] On both types of tumor cells, pretreatment with Neu (or Neu@MG) prior to NK cell incubation leads to a higher cytotoxicity without cell type bias, verifying the boost effect of tumor cell desialyation on NK cell killing activity. However, sequential

https://dx.doi.org/10.1021/acsami.0c15212
ACS Appl. Mater. Interfaces 2020, 12, 54387−54398

performing Neu@MG@Apt-based Sia trimming and NK cell incubation can only generate an enhanced cytotoxicity toward MDA-MB-231 cells rather than MCF-7 cells, demonstrating the achievement of cell-specific potentiation of the NK cell immune response by the proposed glyco-editing method.

To mimic real complex environment, live MDA-MB-231 and MCF-7 cells are cocultured and subjected to Neu, Neu@MG, or Neu@MG@Apt-based desialylation, followed by NK cell incubation. The cell viability is indicated by calcein-AM (green fluorescence), and the target cells are labeled by TR of Neu@MG@Apt or Apt (red fluorescence). Desialylation treatment without NK cell incubation causes little influence on calcein-AM fluorescence (Figure 6b,c), while just NK cell incubation leads to an obvious decrease of cell viability regardless of cell type. In good agreement with the results obtained in single-cultured cell setting, pretreatment by Neu or Neu@MG prior to NK cell treatment causes a further impaired cell viability on both cell types. However, the cells undergoing Neu@MG@Apt-based Sia trimming and then NK cell incubation (Neu@MG@Apt + NK) can be divided into two classes: the cells with red fluorescence (*i.e.*, MDA-MB-231 cells) display an even weaker green fluorescence compared with those solely treated by NK cells; in contrast, the cells without red fluorescence (*i.e.*, MCF-7 cells) show negligible change. The observation results are also verified by flow cytometry (Figure S14). Taken together, these data demonstrate the feasibility of using the proposed method for cell-specific promotion of antitumor immunity of NK cells and also highlight the opportunity to avoid unnecessary influence on glycans during probe delivery in future *in vivo* study.

CONCLUSIONS

A thermally triggered, *in situ* cell-specific glyco-editing method is developed for regulation of lectin recognition and immune response against target cells. The method realizes spatiotemporal control of glyco-editing event *from the outside of cells* by two means: (1) specific recognition between Apt and target cells for guiding glyco-editing enzyme to the given cell surface; (2) thermally sensitive modulation of the accessibility of glyco-editing enzyme by a cell-compatible, intelligent MG. The thermal regulatory handle endows the strategy with easy operation, excellent cytocompatibility, and more importantly, flexibility for different application scenarios. To afford a research tool for glycan functions (*e.g.*, recognition) on cellular level, just as in this work, the VPTT of the MG (27 °C) ensures the efficient release of the glyco-editing enzyme at 37 °C, which is the most convenient temperature for researchers to perform cultured cell-based experiments. As expected, using cell surface Sia as the trimming object, cell-specific regulation of lectin binding is realized on live target cells in both single- and cocultured settings. This highlights the capability of our method for not only revelation of the functional roles of glycans on a given type of cells in complex biological environments but also modulation of cell recognition behaviors in a cell-specific manner. Our method is also applicable to tissue slices that tumor-specific glyco-editing is achieved, for the first time, on these more representative samples. Inspired by these results, we further demonstrate the feasibility of performing cell-specific Sia trimming to boost the immune response of NK cells against a given type of cultured tumor cells. Thus, our method provides a potentially viable solution for avoiding disturbance from glyco-editing before probe reaching tumor sites. Through optimization of the macromer constitution to adjust VPTT beyond 37 °C[51,52] and combination with photothermal nanomaterials,[53,54] the method could be further updated for tumor-targeted glyco-editing and immunosuppression relief *in vivo* using light stimulus to increase local temperature and trigger Neu release. The proposed method could be readily adapted for other glyco-editing enzymes, thus enabling versatile tailoring of cell surface glycans. Thus, this work will contribute to a deep understanding of cellular glycan recognition of chemical and biological relevance and also pave the way for *in vivo* glycoimmune-checkpoint-targeted precision cancer therapy.

ASSOCIATED CONTENT

Supporting Information

The Supporting Information is available free of charge at https://pubs.acs.org/doi/10.1021/acsami.0c15212.

Experimental section; scheme for preparation of thermally sensitive MG; evaluation of the influence from MG on detection of Neu concentration and Neu activity; effect of temperature on the Neu activity; study of the effects of various components or probes on cell viability; exclusion of the effects of F127, F127-LA, F127-LA-DA, and MG on Neu activity; demonstration of Apt binding specificity of Neu@MG@Apt toward MDA-MB-231 cells; optimization of experimental conditions for Neu@MG@Apt-based Sia trimming; analysis of the average amount of Neu released from cell-bound Neu@MG@Apt per cell; flow cytometric verification of cell-specific glyco-editing in cocultured cell setting; tumor-specific glyco-editing on tissue slices from subcutaneous MDA-MB-231 xenografts and normal breast tissues; demonstration of cell specificity of Neu@MG@Apt-based Sia trimming using bladder tumor tissue slices; demonstration of the successful isolation of NK cells from PBMCs; cell viability of separately cultured MDA-MB-231 and MCF-7 cells after incubation with NK cells; and flow cytometric verification of cell-specific potentiation of NK cell killing activity in cocultured cell setting (PDF)

AUTHOR INFORMATION

Corresponding Author

Lin Ding − *State Key Laboratory of Analytical Chemistry for Life Science, School of Chemistry and Chemical Engineering and Chemistry and Biomedicine Innovation Center (ChemBIC), Nanjing University, Nanjing 210023, China;* orcid.org/0000-0001-5381-3484; Email: dinglin@nju.edu.cn

Authors

Xiaofei Yu − *State Key Laboratory of Analytical Chemistry for Life Science, School of Chemistry and Chemical Engineering, Nanjing University, Nanjing 210023, China*

Huifang Shi − *State Key Laboratory of Analytical Chemistry for Life Science, School of Chemistry and Chemical Engineering, Nanjing University, Nanjing 210023, China*

Yiran Li − *State Key Laboratory of Analytical Chemistry for Life Science, School of Chemistry and Chemical Engineering, Nanjing University, Nanjing 210023, China*

Yuna Guo − *State Key Laboratory of Analytical Chemistry for Life Science, School of Chemistry and Chemical Engineering, Nanjing University, Nanjing 210023, China*

https://dx.doi.org/10.1021/acsami.0c15212
ACS Appl. Mater. Interfaces 2020, 12, 54387−54398

Peiwen Zhang − *State Key Laboratory of Analytical Chemistry for Life Science, School of Chemistry and Chemical Engineering, Nanjing University, Nanjing 210023, China*
Guyu Wang − *State Key Laboratory of Analytical Chemistry for Life Science, School of Chemistry and Chemical Engineering, Nanjing University, Nanjing 210023, China*
Lei Li − *State Key Laboratory of Analytical Chemistry for Life Science, School of Chemistry and Chemical Engineering, Nanjing University, Nanjing 210023, China*
Xian Chen − *Jiangsu Province Blood Center, Nanjing 210008, China*
Huangxian Ju − *State Key Laboratory of Analytical Chemistry for Life Science, School of Chemistry and Chemical Engineering, Nanjing University, Nanjing 210023, China;* orcid.org/0000-0002-6741-5302

Complete contact information is available at: https://pubs.acs.org/10.1021/acsami.0c15212

Author Contributions

L.D., H.J., and X.Y. conceived the projects and designed the experiments. X.Y., H.S., Y.L., Y.G., P.Z., G.W., L.L., and X.C. performed the experiments. All authors have given approval to the final version of the manuscript.

Notes

The authors declare no competing financial interest.

■ ACKNOWLEDGMENTS

We gratefully acknowledge support from the National Natural Science Foundation of China (21974067 and 21675082), the National Key Research and Development Program of China (2018YFC1004704), Fundamental Research Funds for the Central Universities (020514380184), and State Key Laboratory of Analytical Chemistry for Life Science (5431ZZXM1903).

■ REFERENCES

(1) Varki, A. Biological Roles of Glycans. *Glycobiology* **2017**, *27*, 3−49.
(2) Reily, C.; Stewart, T. J.; Renfrow, M. B.; Novak, J. Glycosylation in Health and Disease. *Nat. Rev. Nephrol.* **2019**, *15*, 346−366.
(3) Engle, D. D.; Tiriac, H.; Rivera, K. D.; Pommier, A.; Whalen, S.; Oni, T. E.; Alagesan, B.; Lee, E. J.; Yao, M. A.; Lucito, M. S.; Spielman, B.; Da Silva, B.; Schoepfer, C.; Wright, K.; Creighton, B.; Afinowicz, L.; Yu, K. H.; Grützmann, R.; Aust, D.; Gimotty, P. A.; Pollard, K. S.; Hruban, R. H.; Goggins, M. G.; Pilarsky, C.; Park, Y.; Pappin, D. J.; Hollingsworth, M. A.; Tuveson, D. A. The Glycan CA19-9 Promotes Pancreatitis and Pancreatic Cancer in Mice. *Science* **2019**, *364*, 1156−1162.
(4) Jiang, H.; López-Aguilar, A.; Meng, L.; Gao, Z.; Liu, Y.; Tian, X.; Yu, G.; Ovryn, B.; Moremen, K. W.; Wu, P. Modulating Cell-Surface Receptor Signaling and Ion Channel Functions by in Situ Glycan Editing. *Angew. Chem., Int. Ed.* **2018**, *57*, 967−971.
(5) RodrÍguez, E.; Schetters, S. T. T.; Van Kooyk, Y. The Tumour Glyco-Code as a Novel Immune Checkpoint for Immunotherapy. *Nat. Rev. Immunol.* **2018**, *18*, 204−211.
(6) Hudak, J. E.; Canham, S. M.; Bertozzi, C. R. Glycocalyx Engineering Reveals a Siglec-Based Mechanism for NK Cell Immunoevasion. *Nat. Chem. Biol.* **2014**, *10*, 69−75.
(7) Daly, J.; Carlsten, M.; Odwyer, M. Sugar Free: Novel Immuno Therapeutic Approaches Targeting Siglecs and Sialic Acids to Enhance Natural Killer Cell Cytotoxicity Against Cancer. *Front. Immunol.* **2019**, *10*, 1047.
(8) Rodrigues, E.; Macauley, M. Hypersialylation in Cancer: Modulation of Inflammation and Therapeutic Opportunities. *Cancers* **2018**, *10*, 207−226.
(9) Adams, O. J.; Stanczak, M.; Von Gunten, S.; Laubli, H. Targeting Sialic Acid-Siglec Interactions to Reverse Immune Suppression in Cancer. *Glycobiology* **2017**, *28*, 640−647.
(10) Xiao, H.; Woods, E. C.; Vukojicic, P.; Bertozzi, C. R. Precision Glycocalyx Editing as a Strategy for Cancer Immunotherapy. *Proc. Natl. Acad. Sci. U.S.A.* **2016**, *113*, 10304−10309.
(11) Granovsky, M.; Fata, J.; Pawling, J.; Muller, W. J.; Khokha, R.; Dennis, J. W. Suppression of Tumor Growth and Metastasis in Mgat5-Deficient Mice. *Nat. Med.* **2000**, *6*, 306−312.
(12) Saxon, E.; Bertozzi, C. R. Cell Surface Engineering by a Modified Staudinger Reaction. *Science* **2000**, *287*, 2007−2010.
(13) Prescher, J. A.; Dube, D. H.; Bertozzi, C. R. Chemical Remodelling of Cell Surfaces in Living Animals. *Nature* **2004**, *430*, 873−877.
(14) Wang, H.; Wang, R.; Cai, K.; He, H.; Liu, Y.; Yen, J.; Wang, Z.; Xu, M.; Sun, Y.; Zhou, X.; Yin, Q.; Tang, L.; Dobrucki, I. T.; Dobrucki, L. W.; Chaney, E. J.; Boppart, S. A.; Fan, T. M.; Lezmi, S.; Chen, X.; Yin, L.; Cheng, J. Selective in Vivo Metabolic Cell-Labeling-Mediated Cancer Targeting. *Nat. Chem. Biol.* **2017**, *13*, 415−424.
(15) Sun, Y.; Hong, S.; Xie, R.; Huang, R.; Lei, R.; Cheng, B.; Sun, D.-e.; Du, Y.; Nycholat, C. M.; Paulson, J. C.; Chen, X. Mechanistic Investigation and Multiplexing of Liposome-Assisted Metabolic Glycan Labeling. *J. Am. Chem. Soc.* **2018**, *140*, 3592−3602.
(16) Shim, M. K.; Yoon, H. Y.; Ryu, J. H.; Koo, H.; Lee, S.; Park, J. H.; Kim, J.-H.; Lee, S.; Pomper, M. G.; Kwon, I. C.; Kim, K. Cathepsin B-Specific Metabolic Precursor for in Vivo Tumor-Specific Fluorescence Imaging. *Angew. Chem., Int. Ed.* **2016**, *55*, 14698−14703.
(17) Zheng, T.; Jiang, H.; Gros, M.; Soriano del Amo, D.; Sundaram, S.; Lauvau, G.; Marlow, F.; Liu, Y.; Stanley, P.; Wu, P. Tracking N-Acetyllactosamine on Cell-Surface Glycans In Vivo. *Angew. Chem., Int. Ed.* **2011**, *50*, 4113−4118.
(18) Chaubard, J.-L.; Krishnamurthy, C.; Yi, W.; Smith, D. F.; Hsieh-Wilson, L. C. Chemoenzymatic Probes for Detecting and Imaging Fucose-α(1-2)-Galactose Glycan Biomarkers. *J. Am. Chem. Soc.* **2012**, *134*, 4489−4492.
(19) Mbua, N. E.; Li, X.; Flanagan-Steet, H. R.; Meng, L.; Aoki, K.; Moremen, K. W.; Wolfert, M. A.; Steet, R.; Boons, G.-J. Selective Exo-Enzymatic Labeling of N-Glycans on the Surface of Living Cells by Recombinant ST6Gal I. *Angew. Chem., Int. Ed.* **2013**, *52*, 13012−13015.
(20) Sun, T.; Yu, S.-H.; Zhao, P.; Meng, L.; Moremen, K. W.; Wells, L.; Steet, R.; Boons, G.-J. One-Step Selective Exoenzymatic Labeling (SEEL) Strategy for the Biotinylation and Identification of Glycoproteins of Living Cells. *J. Am. Chem. Soc.* **2016**, *138*, 11575−11582.
(21) Li, J.; Chen, M.; Liu, Z.; Zhang, L.; Felding, B. H.; Moremen, K. W.; Lauvau, G.; Abadier, M.; Ley, K.; Wu, P. A Single-Step Chemoenzymatic Reaction for the Construction of Antibody-Cell Conjugates. *ACS Cent. Sci.* **2018**, *4*, 1633−1641.
(22) Nischan, N.; Kohler, J. J. Advances in Cell Surface Glycoengineering Reveal Biological Function. *Glycobiology* **2016**, *26*, 789−796.
(23) Shearer, R. F.; Saunders, D. N. Experimental Design for Stable Genetic Manipulation in Mammalian Cell Lines: Lentivirus and Alternatives. *Genes Cells* **2015**, *20*, 1−10.
(24) Chang, P. V.; Chen, X.; Smyrniotis, C.; Xenakis, A.; Hu, T.; Bertozzi, C. R.; Wu, P. Metabolic Labeling of Sialic Acids in Living Animals with Alkynyl Sugars. *Angew. Chem., Int. Ed.* **2009**, *48*, 4030−4033.
(25) Qin, W.; Qin, K.; Fan, X.; Peng, L.; Hong, W.; Zhu, Y.; Lv, P.; Du, Y.; Huang, R.; Han, M.; Cheng, B.; Liu, Y.; Zhou, W.; Wang, C.; Chen, X. Artificial Cysteine S-glycosylation Induced by Per-O-Acetylated Unnatural Monosaccharides during Metabolic Glycan Labeling. *Angew. Chem., Int. Ed.* **2018**, *57*, 1817−1820.
(26) Hui, J.; Bao, L.; Li, S.; Zhang, Y.; Feng, Y.; Ding, L.; Ju, H. Localized Chemical Remodeling for Live Cell Imaging of Protein-Specific Glycoform. *Angew. Chem., Int. Ed.* **2017**, *56*, 8139−8143.

(27) Zhang, P.; Li, Y.; Yu, X.; Ju, H.; Ding, L. Switchable Enzymatic Accessibility for Precision Cell-Selective Surface Glycan Remodeling. *Chem.—Eur. J.* **2019**, *25*, 10505−10510.
(28) Gray, M. A.; Stanczak, M. A.; Mantuano, N. R.; Xiao, H.; Pijnenborg, J. F. A.; Malaker, S. A.; Miller, C. L.; Weidenbacher, P. A.; Tanzo, J. T.; Ahn, G.; Woods, E. C.; Läubli, H.; Bertozzi, C. R. Targeted Glycan Degradation Potentiates the Anticancer Immune Response In Vivo. *Nat. Chem. Biol.* **2020**, *16*, 1376.
(29) Li, L.; Jiang, Y.; Cui, C.; Yang, Y.; Zhang, P.; Stewart, K.; Pan, X.; Li, X.; Yang, L.; Qiu, L.; Tan, W. Modulating Aptamer Specificity with pH-Responsive DNA Bonds. *J. Am. Chem. Soc.* **2018**, *140*, 13335−13339.
(30) Brieke, C.; Rohrbach, F.; Gottschalk, A.; Mayer, G.; Heckel, A. Light-Controlled Tools. *Angew. Chem., Int. Ed.* **2012**, *51*, 8446−8476.
(31) Ellis-Davies, G. C. R. Caged Compounds: Photorelease Technology for Control of Cellular Chemistry and Physiology. *Nat. Methods* **2007**, *4*, 619−628.
(32) Zhou, L.; Chen, Z.; Dong, K.; Yin, M.; Ren, J.; Qu, X. DNA-Mediated Construction of Hollow Upconversion Nanoparticles for Protein Harvesting and Near-Infrared Light Triggered Release. *Adv. Mater.* **2014**, *26*, 2424−2430.
(33) Yan, L.; Zhu, Z.; Zou, Y.; Huang, Y.; Liu, D.; Jia, S.; Xu, D.; Wu, M.; Zhou, Y.; Zhou, S.; Yang, C. J. Target-Responsive "Sweet" Hydrogel with Glucometer Readout for Portable and Quantitative Detection of Non-Glucose Targets. *J. Am. Chem. Soc.* **2013**, *135*, 3748−3751.
(34) Zhang, P.; Wang, C.; Zhao, J.; Xiao, A.; Shen, Q.; Li, L.; Li, J.; Zhang, J.; Min, Q.; Chen, J.; Chen, H.-Y.; Zhu, J.-J. Near Infrared-Guided Smart Nanocarriers for Microrna-Controlled Release of Doxorubicin/siRNA with Intracellular ATP as Fuel. *ACS Nano* **2016**, *10*, 3637−3647.
(35) Qing, G.; Zhao, X.; Gong, N.; Chen, J.; Li, X.; Gan, Y.; Wang, Y.; Zhang, Z.; Zhang, Y.; Guo, W.; Luo, Y.; Liang, X. Thermo-Responsive Triple-Function Nanotransporter for Efficient Chemo-Photothermal Therapy of Multidrug-Resistant Bacterial Infection. *Nat. Commun.* **2019**, *10*, 4336.
(36) Pearce, O. M. T.; Läubli, H. Sialic Acids in Cancer Biology and Immunity. *Glycobiology* **2016**, *26*, 111−128.
(37) Pinho, S. S.; Reis, C. A. Glycosylation in Cancer: Mechanisms and Clinical Implications. *Nat. Rev. Cancer* **2015**, *15*, 540−555.
(38) McGrath, R. T.; McKinnon, T. A. J.; Byrne, B.; O'Kennedy, R.; Terraube, V.; McRae, E.; Preston, R. J. S.; Laffan, M. A.; O'Donnell, J. S. Expression of Terminal α2-6-Linked Sialic Acid on Von Willebrand Factor Specifically Enhances Proteolysis by ADAMTS13. *Blood* **2010**, *115*, 2666−2673.
(39) Li, X.; Zhang, W.; Liu, L.; Zhu, Z.; Ouyang, G.; An, Y.; Zhao, C.; Yang, C. J. In Vitro Selection of DNA Aptamers for Metastatic Breast Cancer Cell Recognition and Tissue Imaging. *Anal. Chem.* **2014**, *86*, 6596−6603.
(40) Li, H.; Hah, J.-M.; Lawrence, D. S. Light-Mediated Liberation of Enzymatic Activity: "Small Molecule" Caged Protein Equivalents. *J. Am. Chem. Soc.* **2008**, *130*, 10474−10475.
(41) Ghosh, M.; Song, X. Y.; Mouneimne, G.; Sidani, M.; Lawrence, D. S.; Condeelis, J. S. Cofilin Promotes Actin Polymerization and Defines the Direction of Cell Motility. *Science* **2004**, *304*, 743−746.
(42) Zhang, Y.; Zhu, W.; Wang, B.; Ding, J. A Novel Microgel and Associated Post-Fabrication Encapsulation Technique of Proteins. *J. Controlled Release* **2005**, *105*, 260−268.
(43) Sawhney, A. S.; Pathak, C. P.; Hubbell, J. A. Bioerodible Hydrogels Based on Photopolymerized Poly(Ethylene Glycol)-co-Poly(α-Hydroxy Acid) Diacrylate Macromers. *Macromolecules* **1993**, *26*, 581−587.
(44) Shibuya, N.; Goldstein, I. J.; Broekaert, W. F.; Nsimba-Lubaki, M.; Peeters, B.; Peumans, W. J. The Elderberry (Sambucus nigra L.) Bark Lectin Recognizes the Neu5Ac(α2-6)Gal/GalNAc Sequence. *J. Biol. Chem.* **1987**, *262*, 1596−1601.
(45) Isabelle, P.; Olivier, P.; Claire, M. S.; Julien, G.; Carole, V.; Francois, B.; Christiane, M.; Martine, C. S.; Annie, B.; Nelly, K.; Philippe, C. Integrin $\alpha_v\beta_3$ Expression Confers on Tumor Cells a Greater Propensity to Metastasize to Bone. *FASEB J.* **2002**, *16*, 1266−1268.
(46) Naume, B.; Nonstad, U.; Steinkjer, B.; Funderud, S.; Smeland, E.; Espevik, T. Immunomagnetic Isolation of NK and LAK Cells. *J. Immunol. Methods* **1991**, *136*, 1−9.
(47) Chen, X.; Han, J.; Chu, J.; Zhang, L.; Zhang, J.; Chen, C.; Chen, L.; Wang, Y.; Wang, H.; Yi, L.; Elder, J. B.; Wang, Q.-E.; He, X.; Kaur, B.; Chiocca, E. A.; Yu, J. A Combinational Therapy of EGFR-CAR NK Cells and Oncolytic Herpes Simplex Virus 1 for Breast Cancer Brain Metastases. *Oncotarget* **2016**, *7*, 27764−27777.
(48) Lamas, B.; Goncalves-Mendes, N.; Nachat-Kappes, R.; Rossary, A.; Caldefie-Chezet, F.; Vasson, M.-P.; Farges, M.-C. Leptin Modulates Dose-Dependently the Metabolic and Cytolytic Activities of NK-92 Cells. *J. Cell. Physiol.* **2013**, *228*, 1202−1209.
(49) Min, D.; Lv, X.-b.; Wang, X.; Zhang, B.; Meng, W.; Yu, F.; Hu, H. Downregulation of miR-302c and miR-520c by 1,25$(OH)_2D_3$ Treatment Enhances the Susceptibility of Tumour Cells to Natural Killer Cell-Mediated Cytotoxicity. *Br. J. Cancer* **2013**, *109*, 723−730.
(50) Lanier, L. L. Up on the Tightrope: Natural Killer Cell Activation and Inhibition. *Nat. Immunol.* **2008**, *9*, 495−502.
(51) Tang, Z.; Weng, J.; Guan, Y.; Zhang, Y. Unexpected Large Depression of VPTT of a PNIPAM Microgel by Low Concentration of PVA. *Macromol. Chem. Phys.* **2017**, *218*, 1700364.
(52) Liu, P.; Luo, Q.; Guan, Y.; Zhang, Y. Drug Release Kinetics from Monolayer Films of Glucose-Sensitive Microgel. *Polymer* **2010**, *51*, 2668−2675.
(53) Tian, Q.; Tang, M.; Sun, Y.; Zou, R.; Chen, Z.; Zhu, M.; Yang, S.; Wang, J.; Wang, J.; Hu, J. Hydrophilic Flower-Like CuS Superstructures as an Efficient 980 nm Laser-Driven Photothermal Agent for Ablation of Cancer Cells. *Adv. Mater.* **2011**, *23*, 3542−3547.
(54) Yin, D.; Li, X.; Ma, Y.; Liu, Z. Targeted Cancer Imaging and Photothermal Therapy via Monosaccharide-Imprinted Gold Nanorods. *Chem. Commun.* **2017**, *53*, 6716−6719.

https://dx.doi.org/10.1021/acsami.0c15212
ACS Appl. Mater. Interfaces 2020, 12, 54387−54398